Measurement of the mass difference $m(D_s^+) - m(D^+)$ at CDF II

D. Acosta,[14] T. Affolder,[7] M. H. Ahn,[25] T. Akimoto,[52] M. G. Albrow,[13] B. Alcorn,[13] C. Alexander,[40] D. Allen,[13] D. Allspach,[13] P. Amaral,[10] D. Ambrose,[40] S. R. Amendolia,[41] D. Amidei,[30] J. Amundson,[13] A. Anastassov,[47] J. Anderson,[13] K. Anikeev,[29] A. Annovi,[41] J. Antos,[1] M. Aoki,[52] G. Apollinari,[13] J.-F. Arguin,[50] T. Arisawa,[54] A. Artikov,[11] T. Asakawa,[52] W. Ashmanskas,[10] A. Attal,[6] C. Avanzini,[41] F. Azfar,[38] P. Azzi-Bacchetta,[39] M. Babik,[13] N. Bacchetta,[39] H. Bachacou,[26] W. Badgett,[13] S. Bailey,[18] J. Bakken,[13] A. Barbaro-Galtieri,[26] A. Bardi,[41] M. Bari,[51] G. Barker,[23] V. E. Barnes,[43] B. A. Barnett,[22] S. Baroiant,[5] M. Barone,[15] E. Barsotti,[13] A. Basti,[41] G. Bauer,[29] D. Beckner,[13] F. Bedeschi,[41] S. Behari,[22] S. Belforte,[51] W. H. Bell,[17] G. Bellendir,[13] G. Bellettini,[41] J. Bellinger,[55] D. Benjamin,[12] A. Beretvas,[13] B. Berg,[35] A. Bhatti,[45] M. Binkley,[13] D. Bisello,[39] M. Bishai,[13] R. E. Blair,[2] C. Blocker,[4] K. Bloom,[30] B. Blumenfeld,[22] A. Bocci,[45] A. Bodek,[44] M. Bogdan,[10] G. Bolla,[43] A. Bolshov,[29] P. S. L. Booth,[27] D. Bortoletto,[43] J. Boudreau,[42] S. Bourov,[13] M. Bowden,[13] D. Box,[13] C. Bromberg,[31] W. Brown,[13] M. Brozovic,[12] E. Brubaker,[26] L. Buckley-Geer,[13] J. Budagov,[11] H. S. Budd,[44] K. Burkett,[18] G. Busetto,[39] P. Bussey,[17] A. Byon-Wagner,[13] K. L. Byrum,[2] S. Cabrera,[12] P. Calafiura,[26] M. Campanelli,[16] M. Campbell,[30] P. Canal,[13] A. Canepa,[43] W. Carithers,[26] D. Carlsmith,[55] R. Carosi,[41] K. Carrell,[49] H. Carter,[13] W. Caskey,[5] A. Castro,[3] D. Cauz,[51] A. Cerri,[26] C. Cerri,[41] L. Cerrito,[21] J. T. Chandler,[56] J. Chapman,[30] S. Chappa,[13] C. Chen,[40] Y. C. Chen,[1] M. T. Cheng,[13] M. Chertok,[5] G. Chiarelli,[41] I. Chirikov-Zorin,[11] G. Chlachidze,[11] F. Chlebana,[13] I. Cho,[25] K. Cho,[25] D. Chokheli,[11] M. L. Chu,[1] J. Y. Chung,[35] W.-H. Chung,[55] Y. S. Chung,[44] C. I. Ciobanu,[21] M. A. Ciocci,[41] S. Cisko,[13] A. G. Clark,[16] M. Coca,[44] K. Coiley,[13] A. P. Colijn,[13] R. Colombo,[13] A. Connolly,[26] M. Convery,[45] J. Conway,[47] G. Cooper,[13] M. Cordelli,[15] G. Cortiana,[39] J. Cranshaw,[49] R. Cudzewicz,[13] R. Culbertson,[13] C. Currat,[26] D. Cyr,[55] D. Dagenhart,[4] L. DalMonte,[13] S. DaRonco,[39] S. D'Auria,[17] R. Davila,[13] J. Dawson,[2] T. Dawson,[13] P. de Barbaro,[44] C. DeBaun,[13] S. De Cecco,[46] S. Dell'Agnello,[15] M. Dell'Orso,[41] R. DeMaat,[13] P. Demar,[13] S. Demers,[44] L. Demortier,[45] M. Deninno,[3] D. De Pedis,[46] P. F. Derwent,[13] G. Derylo,[13] T. Devlin,[47] C. Dionisi,[46] J. R. Dittmann,[13] P. Doksus,[21] A. Dominguez,[26] S. Donati,[41] F. Donno,[41] M. D'Onofrio,[16] T. Dorigo,[39] R. Downing,[21] G. Drake,[2] C. Drennan,[13] V. Drollinger,[33] I. Dunietz,[13] A. Dyer,[13] K. Ebina,[54] N. Eddy,[21] R. Ely,[26] E. Engels, Jr.,[42] R. Erbacher,[13] M. Erdmann,[23] D. Errede,[21] S. Errede,[21] R. Eusebi,[44] H.-C. Fang,[26] S. Farrington,[17] R. G. Feild,[56] M. Feindt,[23] J. P. Fernandez,[43] C. Ferretti,[30] R. D. Field,[14] I. Fiori,[41] M. Fischler,[13] G. Flanagan,[31] B. Flaugher,[13] L. R. Flores-Castillo,[42] A. Foland,[18] S. Forrester,[5] G. W. Foster,[13] M. Franklin,[18] H. Frisch,[10] J. Fromm,[13] Y. Fujii,[24] I. Furic,[29] I. Furic,[29] G. Galeotti,[41] G. Galet,[39] A. Gallas,[34] M. Gallinaro,[45] O. Ganel,[49] C. Garcia,[35] M. Garcia-Sciveres,[26] A. F. Garfinkel,[43] M. Garwacki,[13,*] G. Garzoglio,[13] C. Gay,[56] H. Gerberich,[12] D. W. Gerdes,[30] E. Gerchtein,[9] J. Gerstenslager,[35] L. Giacchetti,[13] S. Giagu,[46] P. Giannetti,[41] A. Gibson,[26] G. Gillespie, Jr.,[13] C. Gingu,[13] C. Ginsburg,[55] K. Giolo,[43] M. Giordani,[5] V. Glagolev,[11] D. Glenzinski,[13] R. Glossen,[13] M. Gold,[33] N. Goldschmidt,[30] D. Goldstein,[6] J. Goldstein,[13] G. Gomez,[8] M. Goncharov,[48] H. Gonzalez,[13] S. Gordon,[13] I. Gorelov,[33] A. T. Goshaw,[12] Y. Gotra,[42] K. Goulianos,[45] J. Grado,[13] M. Gregori,[51] A. Gresele,[3] T. Griffin,[13] G. Grim,[5] C. Grimm,[13] S. Gromoll,[29] C. Grosso-Pilcher,[10] C. Gu,[49] V. Guarino,[2] M. Guenther,[43] J. Guimaraes da Costa,[18] C. Haber,[26] A. Hahn,[13] K. Hahn,[40] S. R. Hahn,[13] E. Halkiadakis,[44] C. Hall,[18] R. Handler,[55] M. Haney,[21] W. Hao,[49] F. Happacher,[15] K. Hara,[52] M. Hare,[53] R. F. Harr,[30] J. Harrington,[13] R. M. Harris,[13] F. Hartmann,[23] K. Hatakeyama,[45] J. Hauser,[6] T. Hawke,[13] C. Hays,[12] E. Heider,[53] B. Heinemann,[27] J. Heinrich,[40] A. Heiss,[23] R. Herber,[13] M. Herndon,[22] M. Herren,[13] D. Hicks,[13] C. Hill,[7] D. Hirschbuehl,[23] A. Hocker,[44] J. Hoff,[13] K. D. Hoffman,[10] J. Hoftiezer,[35] A. Holloway,[18] L. Holloway,[21] S. Holm,[13] D. Holmgren,[13] S. Hou,[1] M. A. Houlden,[27] J. Howell,[13] M. Hrycyk,[13] P. Hubbard,[13] R. E. Hughes,[35] B. T. Huffman,[38] J. Humbert,[13] J. Huston,[31] K. Ikado,[55] J. Incandela,[7] G. Introzzi,[41] M. Iori,[46] I. Ishizawa,[52] C. Issever,[7] A. Ivanov,[44] Y. Iwata,[20] B. Iyutin,[29] E. James,[30] D. Jang,[47] J. Jarrell,[33] D. Jeans,[46] H. Jensen,[13] R. Jetton,[13] M. Johnson,[35] M. Jones,[40] T. Jones,[13] S. Y. Jun,[9] T. Junk,[21] J. Kallenbach,[13] T. Kamon,[48] J. Kang,[30] M. Karagoz Unel,[34] P. E. Karchin,[30] S. Kartal,[13] H. Kasha,[56] M. Kasten,[21] Y. Kato,[37] Y. Kemp,[23] R. D. Kennedy,[13] K. Kephart,[13] R. Kephart,[13] D. Khazins,[12] V. Khotilovich,[48] B. Kilminster,[44] B. J. Kim,[25] D. H. Kim,[25] H. S. Kim,[21] J. Kim,[25] M. J. Kim,[9] M. S. Kim,[25] S. B. Kim,[25] S. H. Kim,[52] T. H. Kim,[29] Y. K. Kim,[10] B. T. King,[27] M. Kirby,[12] M. Kirk,[4] L. Kirsch,[4] R. Klein,[13] S. Klimenko,[14] M. Knapp,[13] D. Knoblauch,[23] B. Knuteson,[10] H. Kobayashi,[52] P. Koehn,[35] K. Kondo,[54] D. J. Kong,[25] J. Konigsberg,[14] W. Kononenko,[40] K. Kordas,[50] A. Korn,[29] A. Korytov,[14] K. Kotelnikov,[32] A. Kotwal,[12] A. Kovalev,[40] J. Kowalkowski,[13] J. Kraus,[21] I. Kravchenko,[29] A. Kreymer,[13] J. Kroll,[40] M. Kruse,[12] V. Krutelyov,[48] S. E. Kuhlmann,[2] A. Kumar,[13] N. Kuznetsova,[13] A. T. Laasanen,[43] S. Lai,[50] S. Lami,[45] S. Lammel,[13] D. Lamore,[13] J. Lancaster,[12] M. Lancaster,[28] R. Lander,[5] G. Lanfranco,[13] K. Lannon,[21] A. Lath,[47] G. Latino,[33] R. Lauhakangas,[19] I. Lazzizzera,[39] Y. Le,[22] T. LeCompte,[2] J. Lee,[25] J. Lee,[44] K. Lee,[49] S. W. Lee,[48] C. M. Lei,[13] M. Leininger,[13] G. L. Leonardi,[13] N. Leonardo,[29] S. Leone,[41] T. Levshina,[13] F. Lewis,[13] J. D. Lewis,[13] K. Li,[56] C. S. Lin,[13] M. Lindgren,[6] T. M. Liss,[21] D. O. Litvintsev,[13] T. Liu,[13] Y. Liu,[16] O. Lobban,[49] N. S. Lockyer,[40] A. Loginov,[32] J. Loken,[38] M. Loreti,[39] J. Loskot,[13] P. F. Loverre,[46] D. Lucchesi,[39] P. Lukens,[13] P. Lutz,[13] L. Lyons,[38] J. Lys,[26] J. MacNerland,[13] D. MacQueen,[50] A. Madorsky,[14] R. Madrak,[18] K. Maeshima,[13] P. Maksimovic,[22] L. Malferrari,[3] P. Mammini,[41] G. Manca,[38] I. Mandrichenko,[13] C. Manea,[39] R. Marginean,[35] J. Marrafino,[13] A. Martin,[56] M. Martin,[22] V. Martin,[34] M. Martínez,[13] T. Maruyama,[10] H. Matsunaga,[52] J. Mayer,[50] G. M. Mayers,[40] P. Mazzanti,[3] K. S. McFarland,[44] D. McGivern,[28] P. M. McIntyre,[48] P. McNamara,[47] R. McNulty,[27] S. Menzemer,[23] A. Menzione,[41] P. Merkel,[13] C. Mesropian,[45] A. Messina,[46] A. Meyer,[13] T. Miao,[13] N. Michael,[13] J. S. Miller,[30] L. Miller,[18] R. Miller,[31] R. Miquel,[26] S. Miscetti,[15] G. Mitselmakher,[14] A. Miyamoto,[24] Y. Miyazaki,[37]

D. Mizicko,[13,*] S. Moccia,[13] A. Moggi,[41] N. Moggi,[3] S. Montero,[12] R. Moore,[13] T. Moore,[21] L. Morris,[13] F. Morsani,[41] T. Moulik,[43] A. Mukherjee,[13] M. Mulhearn,[29] T. Muller,[23] R. Mumford,[22] A. Munar,[40] P. Murat,[13] S. Murgia,[31] J. Nachtman,[13] V. Nagaslaev,[49] S. Nahn,[56] I. Nakamura,[40] I. Nakano,[36] A. Napier,[53] R. Napora,[22] V. Necula,[14] C. Nelson,[13] T. Nelson,[13] C. Neu,[35] M. S. Neubauer,[29] D. Neuberger,[23] W. Newby,[13] F. M. Newcomer,[40] C. Newman-Holmes,[13] F. Niell,[30] J. Nielsen,[26] A.-S. Nicollerat,[16] T. Nigmanov,[42] H. Niu,[4] L. Nodulman,[2] W. Noe, Jr.,[13] K. Oesterberg,[19] T. Ogawa,[54] S. Oh,[12] Y. D. Oh,[25] K. Ohl,[56] T. Ohsugi,[20] R. Oishi,[52] T. Okusawa,[37] R. Oldeman,[40] R. Orava,[19] W. Orejudos,[26] S. Orr,[13] G. Pagani,[41] C. Pagliarone,[41] F. Palmonari,[41] I. Ramos,[13] S. Panacek,[13] D. Pantano,[39] R. Paoletti,[41] V. Papadimitriou,[49] R. Pasetes,[13] S. Pashapour,[50] D. Passuello,[41] M. Paterno,[13] J. Patrick,[13] G. Pauletta,[51] M. Paulini,[9] T. Pauly,[38] C. Paus,[29] V. Pavlicek,[13] S. Pavlon,[29] D. Pellett,[5] A. Penzo,[51] B. Perington,[13] G. Petragnani,[41] D. Petravick,[13] T. J. Phillips,[12] F. Photos,[15] G. Piacentino,[41] C. Picciolo,[13] L. Piccoli,[13] J. Piedra,[8] K. T. Pitts,[21] R. Plunkett,[13] A. Pompoš,[43] L. Pondrom,[55] G. Pope,[42] O. Poukhov,[11] F. Prakoshyn,[11] T. Pratt,[27] A. Profeti,[41] A. Pronko,[14] J. Proudfoot,[2] G. Punzi,[41] J. Rademacker,[38] F. Rafaelli,[41] A. Rakitine,[29] S. Rappoccio,[18] F. Ratnikov,[47] J. Rauch,[13] H. Ray,[30] R. Rechenmacher,[13] S. Reia,[51] A. Reichold,[38] V. Rekovic,[33] P. Renton,[38] M. Rescigno,[46] F. Rimondi,[3] K. Rinnert,[23] L. Ristori,[41] M. Riveline,[50] C. Rivetta,[13] W. J. Robertson,[12] A. Robson,[38] T. Rodrigo,[8] S. Rolli,[53] M. Roman,[13] S. Rosenberg,[13] L. Rosenson,[29] R. Roser,[13] R. Rossin,[39] C. Rott,[43] A. Ruiz,[8] J. Russ,[9] D. Ryan,[53] H. Saarikko,[19] S. Sabik,[50] L. Sadler,[13] A. Safonov,[5] R. St. Denis,[17] W. K. Sakumoto,[44] D. Saltzberg,[6] C. Sanchez,[35] H. Sanders,[10] R. Sanders,[13] M. Sandrew,[35] A. Sansoni,[15] L. Santi,[51] S. Sarkar,[46] H. Sarraj,[13] J. Sarraj,[13] H. Sato,[52] P. Savard,[50] P. Schemitz,[23] P. Schlabach,[13] E. E. Schmidt,[13] J. Schmidt,[13] M. P. Schmidt,[56] M. Schmitt,[34] R. Schmitt,[13] M. Schmitz,[13] G. Schofield,[5] K. Schuh,[13] K. Schultz,[13] L. Scodellaro,[39] L. Scott,[13] A. Scribano,[41] F. Scuri,[41] A. Sedov,[43] S. Segler,[13,*] S. Seidel,[33] Y. Seiya,[52] A. Semenov,[11] F. Semeria,[3] L. Sexton-Kennedy,[13] I. Sfiligoi,[15] J. Shallenberger,[13] M. D. Shapiro,[26] T. Shaw,[13] T. Shears,[27] A. Shenai,[13] P. F. Shepard,[42] M. Shimojima,[52] M. Shochet,[10] Y. Shon,[55] M. Shoun,[13] A. Sidoti,[41] J. Siegrist,[26] C. Sieh,[13] M. Siket,[1] A. Sill,[49] R. Silva,[13] V. Simaitis,[21] P. Sinervo,[50] I. Sirotenko,[13] A. Sisakyan,[11] A. Skiba,[23] A. J. Slaughter,[13] K. Sliwa,[53] J. Smith,[5] F. D. Snider,[13] R. Snihur,[28] S. V. Somalwar,[47] J. Spalding,[13] M. Spezziga,[49] L. Spiegel,[13] F. Spinella,[41] M. Spiropulu,[10] H. Stadie,[23] R. Stanek,[13] N. Stanfield,[13] B. Stelzer,[50] O. Stelzer-Chilton,[50] J. Strologas,[21] D. Stuart,[7] W. Stuermer,[13] A. Sukhanov,[14] K. Sumorok,[29] H. Sun,[53] T. Suzuki,[52] J. Syu,[13] A. Szymulanski,[13] A. Taffard,[27] S. F. Takach,[30] H. Takano,[52] R. Takashima,[20] Y. Takeuchi,[52] K. Takikawa,[52] P. Tamburello,[12] M. Tanaka,[2] R. Tanaka,[36] D. Tang,[13] N. Tanimoto,[36] B. Tannenbaum,[6] S. Tapprogge,[19] R. D. Taylor,[13] G. Teafoe,[13] M. Tecchio,[30] P. K. Teng,[1] K. Terashi,[45] T. Terentieva,[13] R. J. Tesarek,[13] S. Tether,[29] J. Thom,[13] A. Thomas,[13] A. S. Thompson,[17] E. Thomson,[35] R. Thurman-Keup,[2] S. Timm,[13] P. Tipton,[44] S. Tkaczyk,[13] D. Toback,[48] K. Tollefson,[31] D. Tonelli,[41] M. Tonnesmann,[31] D. Torretta,[13] C. Trimby,[13] W. Trischuk,[50] J. Trumbo,[13] J. Tseng,[29] R. Tsuchiya,[54] S. Tsuno,[52] D. Tsybychev,[14] N. Turini,[41] M. Turner,[27] F. Ukegawa,[52] T. Unverhau,[17] S. Uozumi,[52] D. Usynin,[40] L. Vacavant,[26] T. Vaiciulis,[44] R. Van Berg,[40] A. Varganov,[30] E. Vataga,[41] S. Vejcik III,[13] G. Velev,[13] G. Veramendi,[26] T. Vickey,[21] R. Vidal,[13] I. Vila,[8] R. Vilar,[8] M. Vittone,[13] J. Voirin,[13] B. Vollmer,[13] I. Vollrath,[50] I. Volobouev,[26] M. von der Mey,[6] M. Votava,[13] R. G. Wagner,[2] R. L. Wagner,[13] W. Wagner,[23] N. Wallace,[47] T. Walter,[23] A. Walters,[13] Z. Wan,[47] A. Wandersee,[56] M. J. Wang,[1] S. M. Wang,[14] B. Ward,[17] S. Waschke,[17] D. Waters,[28] T. Watts,[47] M. Weber,[26] L. Weems,[13] H. Wenzel,[23] W. Wester,[13] B. Whitehouse,[53] W. Wickenberg,[13] A. B. Wicklund,[2] E. Wicklund,[13] R. Wigmans,[49] C. Wike,[13] T. Wilkes,[5] H. H. Williams,[40] P. Wilson,[13] B. L. Winer,[35] P. Wittich,[40] S. Wolbers,[13] M. Wolter,[53] M. Wong,[13] M. Worcester,[6] R. Worland,[13] S. Worm,[47] T. Wright,[30] J. Wu,[13] X. Wu,[16] F. Würthwein,[29] A. Wyatt,[28] A. Yagil,[13] K. Yamamoto,[37] T. Yamashita,[36] U. K. Yang,[10] W. Yao,[26] R. Yarema,[13] G. P. Yeh,[13] K. Yi,[22] D. Yocum,[13] J. Yoh,[13] P. Yoon,[44] K. Yorita,[54] T. Yoshida,[37] I. Yu,[25] S. Yu,[40] Z. Yu,[56] J. C. Yun,[13] M. Zalokar,[13] L. Zanello,[46] A. Zanetti,[51] I. Zaw,[18] F. Zetti,[41] J. Zhou,[47] T. Zimmerman,[13] A. Zsenei,[16] and S. Zucchelli[3]

(CDF II Collaboration)

[1]*Institute of Physics, Academia Sinica, Taipei, Taiwan 11529, Republic of China*
[2]*Argonne National Laboratory, Argonne, Illinois 60439, USA*
[3]*Istituto Nazionale di Fisica Nucleare, University of Bologna, I-40127 Bologna, Italy*
[4]*Brandeis University, Waltham, Massachusetts 02254, USA*
[5]*University of California at Davis, Davis, California 95616, USA*
[6]*University of California at Los Angeles, Los Angeles, California 90024, USA*
[7]*University of California at Santa Barbara, Santa Barbara, California 93106, USA*
[8]*Instituto de Fisica de Cantabria, CSIC–University of Cantabria, 39005 Santander, Spain*
[9]*Carnegie Mellon University, Pittsburgh, Pennsylvania 15213, USA*
[10]*Enrico Fermi Institute, University of Chicago, Chicago, Illinois 60637, USA*
[11]*Joint Institute for Nuclear Research, RU-141980 Dubna, Russia*
[12]*Duke University, Durham, North Carolina 27708, USA*
[13]*Fermi National Accelerator Laboratory, Batavia, Illinois 60510, USA*
[14]*University of Florida, Gainesville, Florida 32611, USA*
[15]*Laboratori Nazionali di Frascati, Istituto Nazionale di Fisica Nucleare, I-00044 Frascati, Italy*
[16]*University of Geneva, CH-1211 Geneva 4, Switzerland*
[17]*Glasgow University, Glasgow G12 8QQ, United Kingdom*

[18]*Harvard University, Cambridge, Massachusetts 02138, USA*
[19]*University of Helsinki, FIN-00044, Helsinki, Finland*
[20]*Hiroshima University, Higashi-Hiroshima 724, Japan*
[21]*University of Illinois, Urbana, Illinois 61801, USA*
[22]*The Johns Hopkins University, Baltimore, Maryland 21218, USA*
[23]*Institut für Experimentelle Kernphysik, Universität Karlsruhe, 76128 Karlsruhe, Germany*
[24]*High Energy Accelerator Research Organization (KEK), Tsukuba, Ibaraki 305, Japan*
[25]*Center for High Energy Physics: Kyungpook National University, Taegu 702-701,*
Seoul National University, Seoul 151-742, Korea,
and SungKyunKwan University, Suwon 440-746, Korea
[26]*Ernest Orlando Lawrence Berkeley National Laboratory, Berkeley, California 94720, USA*
[27]*University of Liverpool, Liverpool L69 7ZE, United Kingdom*
[28]*University College London, London WC1E 6BT, United Kingdom*
[29]*Massachusetts Institute of Technology, Cambridge, Massachusetts 02139, USA*
[30]*University of Michigan, Ann Arbor, Michigan 48109, USA*
[31]*Michigan State University, East Lansing, Michigan 48824, USA*
[32]*Institution for Theoretical and Experimental Physics, ITEP, Moscow 117259, Russia*
[33]*University of New Mexico, Albuquerque, New Mexico 87131, USA*
[34]*Northwestern University, Evanston, Illinois 60208, USA*
[35]*The Ohio State University, Columbus, Ohio 43210, USA*
[36]*Okayama University, Okayama 700-8530, Japan*
[37]*Osaka City University, Osaka 588, Japan*
[38]*University of Oxford, Oxford OX1 3RH, United Kingdom*
[39]*Universitá di Padova, Istituto Nazionale di Fisica Nucleare, Sezione di Padova-Trento, I-35131 Padova, Italy*
[40]*University of Pennsylvania, Philadelphia, Pennsylvania 19104, USA*
[41]*Istituto Nazionale di Fisica Nucleare, University and Scuola Normale Superiore of Pisa, I-56100 Pisa, Italy*
[42]*University of Pittsburgh, Pittsburgh, Pennsylvania 15260, USA*
[43]*Purdue University, West Lafayette, Indiana 47907, USA*
[44]*University of Rochester, Rochester, New York 14627, USA*
[45]*Rockefeller University, New York, New York 10021, USA*
[46]*Instituto Nazionale de Fisica Nucleare, Sezione di Roma, University di Roma I, "La Sapienza," I-00185 Roma, Italy*
[47]*Rutgers University, Piscataway, New Jersey 08855, USA*
[48]*Texas A&M University, College Station, Texas 77843, USA*
[49]*Texas Tech University, Lubbock, Texas 79409, USA*
[50]*Institute of Particle Physics, University of Toronto, Toronto M5S 1A7, Canada*
[51]*Istituto Nazionale di Fisica Nucleare, University of Trieste/Udine, Italy*
[52]*University of Tsukuba, Tsukuba, Ibaraki 305, Japan*
[53]*Tufts University, Medford, Massachusetts 02155, USA*
[54]*Waseda University, Tokyo 169, Japan*
[55]*University of Wisconsin, Madison, Wisconsin 53706, USA*
[56]*Yale University, New Haven, Connecticut 06520, USA*

We present a measurement of the mass difference $m(D_s^+) - m(D^+)$, where both the D_s^+ and D^+ are reconstructed in the $\phi\pi^+$ decay channel. This measurement uses 11.6 pb^{-1} of data collected by CDF II using the new displaced-track trigger. The mass difference is found to be $m(D_s^+) - m(D^+) = 99.41 \pm 0.38$(stat) ± 0.21(syst) MeV/c^2.

I. INTRODUCTION

Meson masses are predicted by different models of quark interactions and the interquark potential. Analytically, the spectrum of heavy-light mesons can be described in the QCD framework using the principles of heavy quark symmetry and heavy quark effective theory [1,2]. These theories state that in the limit of infinitely heavy quark mass, the properties of the meson are independent of the heavy quark flavor and that the heavy quark does not contribute to the orbital degrees of freedom. The theory predicts that up to corrections of order $1/m_{b,c}$, $m(B_s^0) - m(B_d^0) = m(D_s^+) - m(D^+)$ [3]. Recently, lattice QCD calculations have also given their predictions for the meson mass spectrum [4–6]. By measuring the masses of mesons precisely, we narrow the range of param-
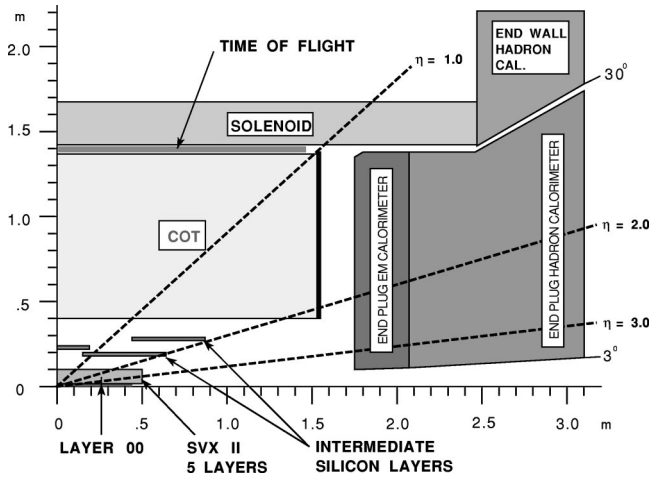
*Deceased.

FIG. 1. Quadrant view of the CDF II integrated tracking system. The Central Outer Tracker (COT) and silicon subdetectors form an integrated tracking system.

eters and approximations that theoretical models use to make predictions. For charm meson masses, a simultaneous fit [7] of all measurements including the mass difference between the D_s^+ and D^+ is used to compare experimental measurements with theoretical predictions. In this paper a measurement of the mass difference $m(D_s^+) - m(D^+)$ in the decay channels $D_s^+ \to \phi \pi^+$ and $D^+ \to \phi \pi^+$ where $\phi \to K^+ K^-$ is presented [8]. The advantage of measuring the mass difference in a common final decay state is that many of the systematic uncertainties cancel. Gathering the large sample of charmed mesons used in this analysis is done using a novel displaced-track trigger, the silicon vertex tracker (SVT) [9], which enables recognition of the decay of long-lived particles early in the trigger system.

II. CDF II DETECTOR AND DATA SET

The data used for this analysis were collected with the upgraded Collider Detector at Fermilab (CDF II) [10] at the Tevatron $p\bar{p}$ collider. The integrated luminosity is 11.6 pb^{-1} at $\sqrt{s} = 1.96$ TeV, taken during the period February–May 2002. These are the first physics-quality data from the run II program.

A. CDF II detector

The CDF II detector is a major upgrade of the original CDF detector which last took data in 1996. The most important aspects of the upgraded detector for this analysis are the new tracking system and the displaced track trigger. CDF II, which is shown in Fig. 1, has an integrated central tracking system immersed in a 1.4-T solenoidal magnetic field for the measurement of charged-particle momenta. The innermost tracking device is a silicon strip vertex detector, which consists of three subdetectors. A single-sided layer of silicon sensors, called layer 00 (L00) [11], is installed directly onto the beryllium vacuum beam pipe, at a radius of 1.7 cm. It is followed by five concentric layers of double-sided silicon sensors (SVXII) [12] located at radii between 2.5 and 10.6

cm. The Intermediate Silicon Layers (ISL) [13] are the outermost silicon subdetector systems, consisting of one double-sided layer at a radius of 22 cm in the central region and two double-sided layers at radii 20 and 28 cm in the forward regions. Surrounding the silicon detector is the Central Outer Tracker (COT) [14], a 3.1-m-long cylindrical open-cell drift chamber covering radii from 40 to 137 cm. The COT is segmented into eight superlayers, each consisting of planes of 12 sense wires. The superlayers alternate between axial wires and wires with a $\pm 2°$ stereo angle, providing three-dimensional tracking. This provides up to 96 position measurements on a track passing through all eight superlayers. A charged particle traversing the tracking volume deposits charge on nearby silicon microstrips (clusters), and signals from the ionization trail in the COT are recorded by the sense wires (hits). Double-sided layers of silicon provide axial (r-φ) measurements of cluster positions on one side and z measurements via small-angle or 90° stereo information on the other. The L00 detector provides r-φ measurements only. COT information and SVXII r-φ information from the SVXII detector are used in this analysis.

B. Tracking parameters

CDF II uses a cylindrical coordinate system (r, φ, z) with the origin at the center of the detector and the z axis along the nominal direction of the proton beam. Tracks are fit to helical trajectories. The plane perpendicular to the beam is referred to as the "transverse plane," and the transverse momentum of the track is referred to as p_T. In the transverse plane, the helix is parametrized with track curvature (C), impact parameter (d_0), and azimuthal angle φ_0. The projection of the track helix onto the transverse plane is a circle of radius r, and the absolute value of the track curvature is $|C| = 1/(2r)$. The sign of the curvature matches the sign of the track charge. The d_0 of a track is another signed variable; its absolute value corresponds to the distance of closest approach of the track to the beam line. The sign of d_0 is taken to be that of $\hat{p} \times \hat{d} \cdot \hat{z}$, where $\hat{p}$ and $\hat{d}$ are unit vectors in the direction of the particle trajectory and the direction of the vector pointing from the primary interaction point to the point of closest approach to the beam, respectively. The angle φ_0 is the azimuthal angle of the particle trajectory at the point of closest approach to the beam. The two remaining parameters that uniquely define the helix in three dimensions are the cotangent of the angle θ between the z axis and the momentum of the particle and z_0, the position along the z axis at the point of closest approach to the beam. The two-dimensional decay length of a D meson L_{xy}^D is defined as

$$L_{xy}^D = \frac{\vec{X}_v \cdot \vec{P}_T^D}{|\vec{P}_T^D|}, \tag{1}$$

where $\vec{P}_T^D$ is the transverse D momentum and $\vec{X}_v$ is the vector pointing from the primary interaction vertex to the D meson decay vertex. We use the average beam position as an estimate of the primary interaction vertex. This is calculated for each data acquisition run. The transverse intensity profile

of the beam is roughly circular and can be approximated by a Gaussian distribution with $\sigma \approx 35 \ \mu$m [15,16].

C. Trigger and data set

CDF II has a three-level trigger system. The first two levels are implemented with custom electronics, while the third is a software trigger based on a version of the final reconstruction software optimized for speed. The most important feature of the trigger system for this analysis is its ability to recognize tracks and vertices displaced from the beam line. A brief description of this part of the trigger system follows. At level 1 of the trigger, the COT provides information to the eXtremely Fast Tracker (XFT) [17], which identifies tracks with $p_T \geq 1.5 \ \text{GeV}/c$. An event passes the level-1 selection if the XFT finds a pair of tracks with opposite charge, such that each has $p_T > 2.0 \ \text{GeV}/c$, the scalar sum of transverse momenta $p_{T1} + p_{T2} > 5.5 \ \text{GeV}/c$, and angular difference $\Delta \varphi_6 < 135°$. The angle φ_6 of a track is defined as the azimuthal angle of the track momentum as measured in superlayer 6 of the COT, which corresponds to a radius of 106 cm from the beamline.

At level 2, the SVT combines XFT track information with SVXII information. Tracks are refit using a linear algorithm, which provides improved φ_0 and p_T measurements. The track impact parameter resolution is about 35 μm [15,16] for tracks with $p_T > 2 \ \text{GeV}/c$. An event passes level-2 selection if there is a track pair reconstructed in the SVT such that each track has $p_T > 2.0 \ \text{GeV}/c$ and $100 \ \mu\text{m} < |d_0| < 1 \ \text{mm}$.

At level 3, the full three-dimensional track fit using COT information is combined with SVT information. The level-2 requirements are confirmed with the improved track measurements. The same tracks that passed the level-1 selection have to pass the level-2 and level-3 requirements. In addition, it is required that the vertex of the two trigger tracks have $L_{xy} > 200 \ \mu$m. The trigger requirements are optimized for selecting multibody decays of long-lived charm and bottom mesons. The optimization is done using an unbiased trigger sample to estimate the background rates and Monte Carlo–simulated events to estimate the signal rates.

Events gathered by the trigger system undergo final ''offline'' event reconstruction with the best available tracking algorithms. In the algorithm used for this measurement, the reconstruction begins with a COT measurement of the track helix. This version of the track is extrapolated into the silicon tracker, starting from the outermost layers and working inward. Based on the uncertainties of the track parameters, a road is formed around the extrapolated trajectory, and only silicon clusters found inside this road are added to the track. As clusters are added, the uncertainties on the track parameters are improved. For this analysis, only the r-φ information of the SVXII detector is used.

III. MOMENTUM SCALE CALIBRATION

The masses of the D_s^+ and D^+ mesons are measured from the momenta of their decay daughters: therefore, it is crucial to calibrate the momentum measurements in the tracking volume. The main effects that are of concern in this analysis
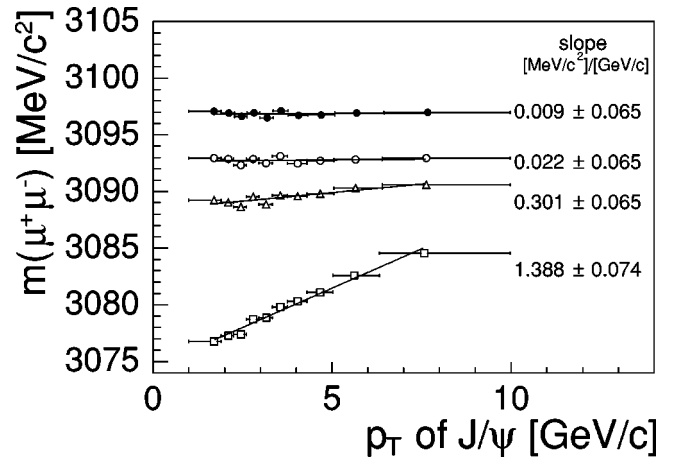

FIG. 2. Dependence of the J/ψ mass on the p_T of the J/ψ. The open squares show the mass dependence for tracks with no energy loss corrections. Open triangles show the result after applying the energy loss for the material accounted for in the GEANT description of the detector. Open circles account for the missing material modeled with the additional layer. Solid circles show the effect of the B field tuning in addition to accounting for all the missing material.

are a proper accounting of the energy loss in detector material and the calibration of the value of the magnetic field (B). Difficulties in accounting for energy loss in the tracking detectors come from an approximate model of the passive material. Uncertainties of the magnetic field are determined directly from the data. The momentum scale calibration for the tracking system is obtained by studying a sample of $\sim 55\,000 J/\psi \rightarrow \mu^+ \mu^-$ decays. An incorrect accounting for material in the detector description causes the reconstructed mass of the J/ψ meson to depend on the its p_T. Using an incorrect magnetic field value when converting track curvature into momentum causes the mass of the J/ψ meson to be shifted. The calibration involves a two-step procedure. In the first step, the dependence of the J/ψ mass on the transverse momentum is eliminated by adding material to the tracking volume description. After that, the magnetic field is calibrated by requiring that the reconstructed $J/\psi \rightarrow \mu^+ \mu^-$ mass be equal to the world average.

A. Procedure

The amount of passive material in the GEANT [18] description of the CDF II silicon tracking volume is adjusted to eliminate the dependence of the invariant mass of the J/ψ candidates on their transverse momentum, as demonstrated in Fig. 2. The missing material is modeled with a layer of uniform thickness located just inside the inner shell of the COT; a layer of $0.56 \pm 0.10 \ \text{g/cm}^2$ eliminates the dependence of the $J/\psi \rightarrow \mu^+ \mu^-$ mass on its p_T. This additional layer corresponds to roughly 20% of the total passive material in the silicon tracking system. Final-state photon radiation causes a tail on the lower end of the J/ψ mass distribution, which distorts (compared with a Gaussian distribution) the shape of the invariant mass distribution. The corresponding
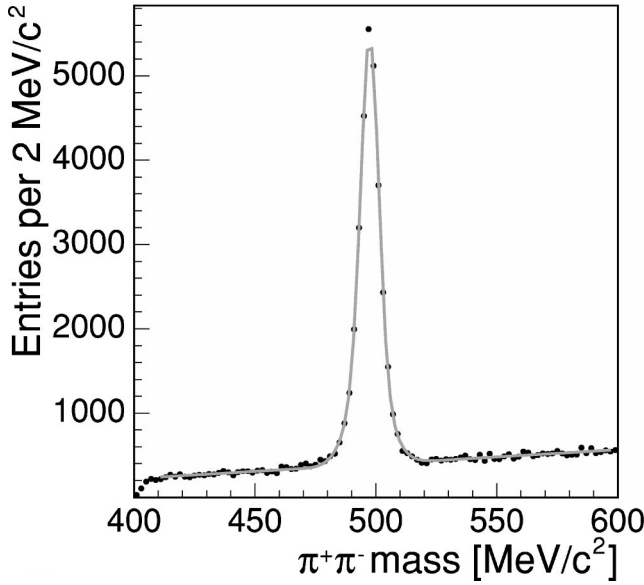
FIG. 3. Measured $\pi^+\pi^-$ mass distribution. A Gaussian distribution and a linear background are fitted to the mass spectrum.

FIG. 4. The $K^-\pi^+$ mass distribution of the reconstructed D^0 candidates. A Gaussian distribution for the signal and a broad Gaussian distribution for the background are fitted to the mass spectrum.

bias is calculated in bins of J/ψ momenta and is taken into account when tuning the amount of passive material in the detector description.

The magnetic field (B) is adjusted to bring the measured $J/\psi \rightarrow \mu^+\mu^-$ mass to the world average value of $m(J/\psi) = 3096.87$ MeV/c^2 [7]. The B field is calibrated to a value of 1.41348 ± 0.00027 T. The precision of the tuning procedure is limited by the number of J/ψ decays available for the calibration.

B. Tests and cross-checks

Several tests and cross-checks are performed to verify the calibration. The J/ψ invariant mass is checked for dependences on the z, φ, and $\cot\theta$ coordinates of the decay in the detector. No significant residual dependence is found after the calibration is applied. The calibration method and parameters—the amount of missing passive material and the magnetic field value—are also cross-checked with other meson decays covering a range of invariant masses. As a check in the low-momentum range, $K_S^0 \rightarrow \pi^+\pi^-$ decays are studied. The $\pi^+\pi^-$ invariant mass distribution is presented in Fig. 3. The K_S^0 decays are also studied for dependences on the radial position of the K_S^0 decay. No significant dependence is found for radii several centimeters inside the silicon detector. The mass of the K_S^0 is checked for run-to-run variations. No significant dependence on the run number is found. Cross-checks with high statistics, corresponding to several ten thousand signal events, are done with samples of $D^0 \rightarrow K^-\pi^+$ and $D^+ \rightarrow K^-\pi^+\pi^+$ decays presented in Figs. 4 and 5, respectively. The D^0 decays are also checked for mass dependence on the p_T of the D^0. Since no particle identification is used, there is a reflection peak in the D^0 mass spectrum coming from the wrong assignment between kaon and pion hypotheses that cannot be removed. The bias due to the reflection peak is estimated using a parametric simulation
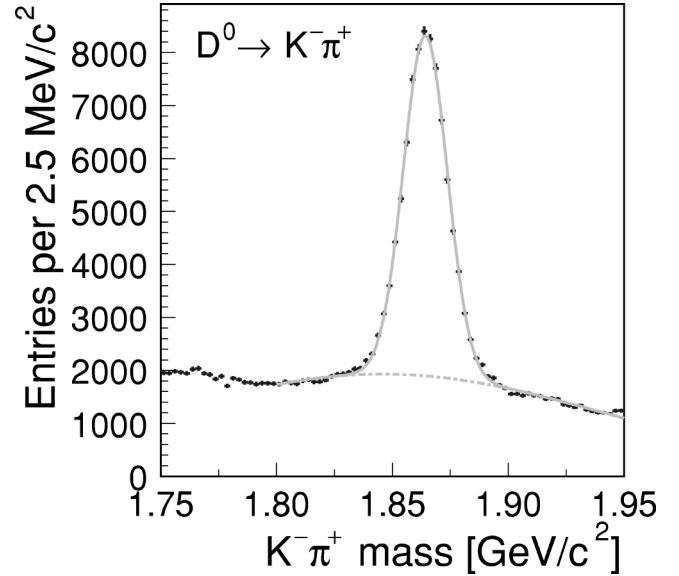
for every p_T bin separately and taken into account in Fig. 6. The $\psi(2S) \rightarrow J/\psi\pi^+\pi^-$ decays are also reconstructed, and the mass distribution is shown in Fig. 7. Finally, a check in the region of higher momenta is done with $\Upsilon \rightarrow \mu^+\mu^-$ decays, presented in Fig. 8. The reconstructed masses are compared to the world average values [7] in Table I. We conclude that the calibration procedure described above accounts well for the energy loss in the silicon tracking volume and applies to a range of reconstructed invariant masses. The calibration
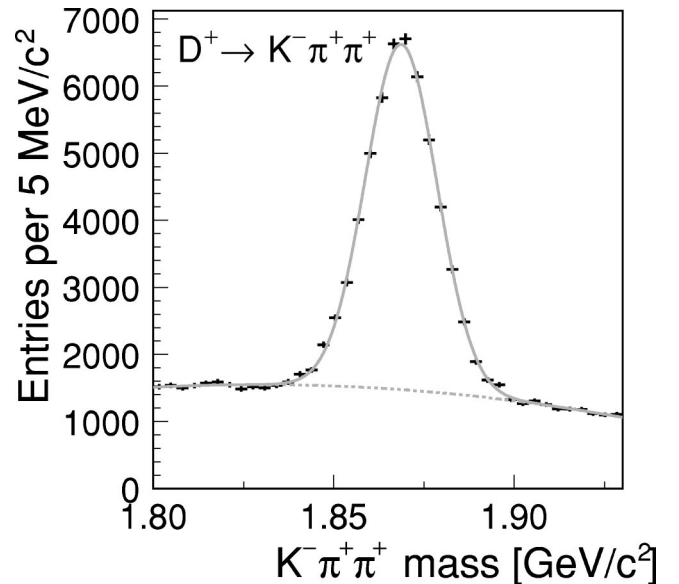

FIG. 5. The $K^-\pi^+\pi^+$ mass distribution of the reconstructed D^+ meson candidates. A Gaussian distribution for the signal and a broad Gaussian distribution for the background are fitted to the mass spectrum.
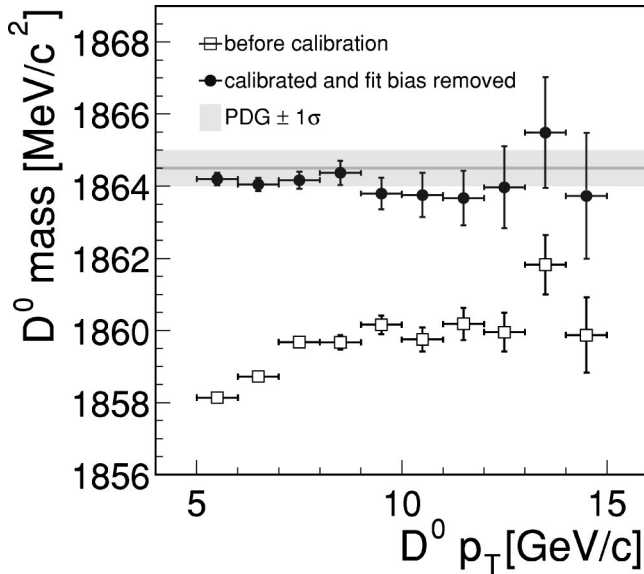
FIG. 6. The dependence of the D^0 mass on its transverse momentum. The open points show mass values before any corrections are applied; the solid points show the dependence after the calibration (energy loss and B field). The systematic bias due to background modeling has been subtracted.

parameters quoted above are used when reconstructing the invariant mass of the D_s^+ and $D^+ \rightarrow \phi\pi$ decays.

One effect is found that is not completely corrected by the calibration. The distribution of the invariant mass of the J/ψ as a function of the curvature difference between the two muons shows a slope, as seen in Fig. 9. This dependence indicates charge-specific effects in the tracker, referred to as "false curvature." It also manifests itself in a difference in mass of the charge conjugates of the same meson. Misalignments in the COT, relative alignment of the COT to the silicon tracker, tilted wire planes, and discrepancies between the COT axis and magnetic field axis can cause such charge dependent false curvature effects. Parametrized corrections

FIG. 7. Measured $\mu^+\mu^-\pi^+\pi^-$ mass distribution for $\psi(2S)$ candidates reconstructed in the $J/\psi\pi^+\pi^-$ decay. A Gaussian distribution and a linear background are fitted to the measured spectrum.
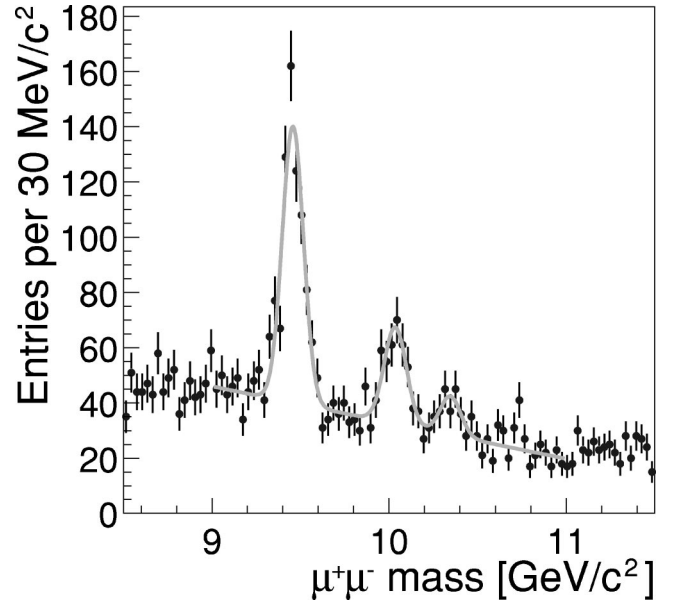

FIG. 8. Measured $\Upsilon \rightarrow \mu^+\mu^-$ mass distribution. Three Gaussian distributions and a linear background are fitted to the mass spectrum.

applied to track parameters improve the distribution shown in Fig. 9. The charge asymmetry of the mass of charged mesons is not eliminated by these corrections. We do not correct for false curvature effects in the calibration procedure, but instead estimate the systematic uncertainty arising from the observed asymmetry.

IV. D_s^+ AND D^+ SELECTION

The D_s^+ and D^+ mesons are selected using offline reconstructed tracks through their decays to $\phi\pi^+$ followed by the subsequent decay $\phi \rightarrow K^+K^-$. To ensure good track quality, the tracks are required to have hits in $\geqslant 20$ COT stereo layers, $\geqslant 20$ axial layers, $\geqslant 3$ silicon r-φ clusters, and $p_T > 400$ MeV/c. No particle identification is used in this analysis, and all mass assignments consistent with the assumed decay are attempted.

The ϕ candidates are selected by requiring two charged tracks, assumed to be kaons, which have opposite charge. The invariant mass of the track pair is required to be within 10 MeV/c^2 of the world average ϕ mass. The detector reso-

TABLE I. Comparison of measured masses of mesons reconstructed using the described calibration parameters and corresponding PDG averages. Uncertainties in reconstructed masses are statistical only.

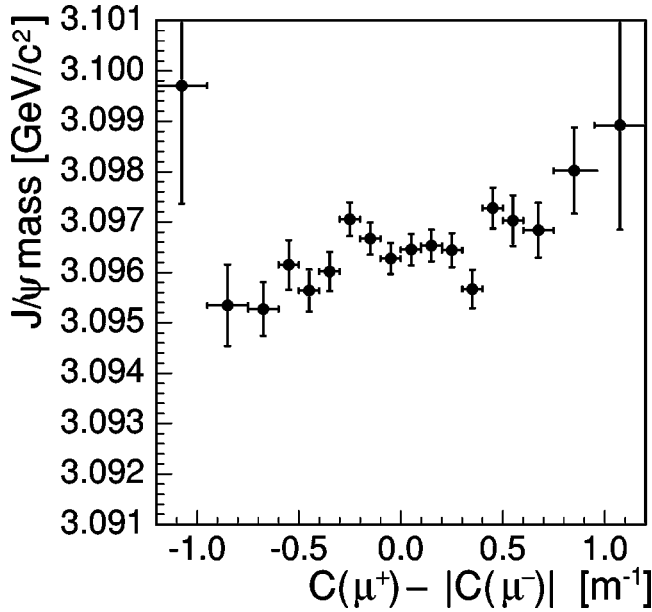| Decay	Mass [MeV/c^2]	PDG [MeV/c^2]
$K_S^0 \rightarrow \pi^+\pi^-$	497.36 ± 0.04	497.672 ± 0.031
$\Upsilon \rightarrow \mu^+\mu^-$	9461 ± 5	9460.30 ± 0.26
$D^0 \rightarrow K^-\pi^+$	1864.15 ± 0.10	1864.5 ± 0.5
$D^+ \rightarrow K^-\pi^+\pi^+$	1868.65 ± 0.07	1869.4 ± 0.5
$\psi(2S) \rightarrow J/\psi\pi^+\pi^-$	3686.43 ± 0.54	3685.96 ± 0.09

FIG. 9. Dependence of the J/ψ mass on the difference of the absolute values of the curvature (C) of the positive and negative muon. This distribution shows a small charge-dependent effect that is not corrected for in the calibration.

lution of the ϕ mass is approximately 4 MeV/c^2. A third track, assumed to be a pion, is added to the ϕ candidate. To avoid using tracks from different interaction vertices, the separation along the beamline of all three tracks—the two kaon candidates and the pion candidate—is required to be <4 cm. Any two of these three tracks satisfy triggerlike criteria using offline quantities: opposite charge, p_T >2.0 GeV/c, and 120 μm<$|d_0|$<1 mm. The third track is only required to have $|d_0|$<2 mm. No further requirements are placed on this track.

All three tracks are constrained to a common vertex in three dimensions. To ensure quality of the vertices, the χ^2 of the vertex in the transverse plane satisfies $\chi^2(r,\varphi)$<7. The displaced-track trigger preferentially accepts events with two-track vertices displaced from the primary interaction point by a few hundred microns. Adding a third track from the primary interaction pulls the three-track vertex toward the beamline, and the resulting L_{xy} of the three-track vertex is much smaller. To eliminate these background candidates, the L_{xy} of the three-track vertex is required to be larger than 500 μm.

The helicity angle (θ_H) is defined as the angle between the ϕ flight direction and the direction of the kaon momentum measured in the ϕ rest frame. The ϕ is polarized in this decay channel, so the helicity angle is expected to follow a $\cos^2\theta_H$ distribution for the signal and a flat distribution for the background. Using sideband subtraction, we verify that the other selection requirements do not distort the shapes of these distributions, as demonstrated in Fig. 10. The helicity angle is required to satisfy $|\cos(\theta_H)|$>0.4.

The requirements on the fit $\chi^2(r,\varphi)$, L_{xy}, and $|\cos(\theta_H)|$ have similar efficiencies. Individually, each requirement is 90%–95% efficient for the signal candidates and rejects 40%–50% of the background. It is unlikely to find two real
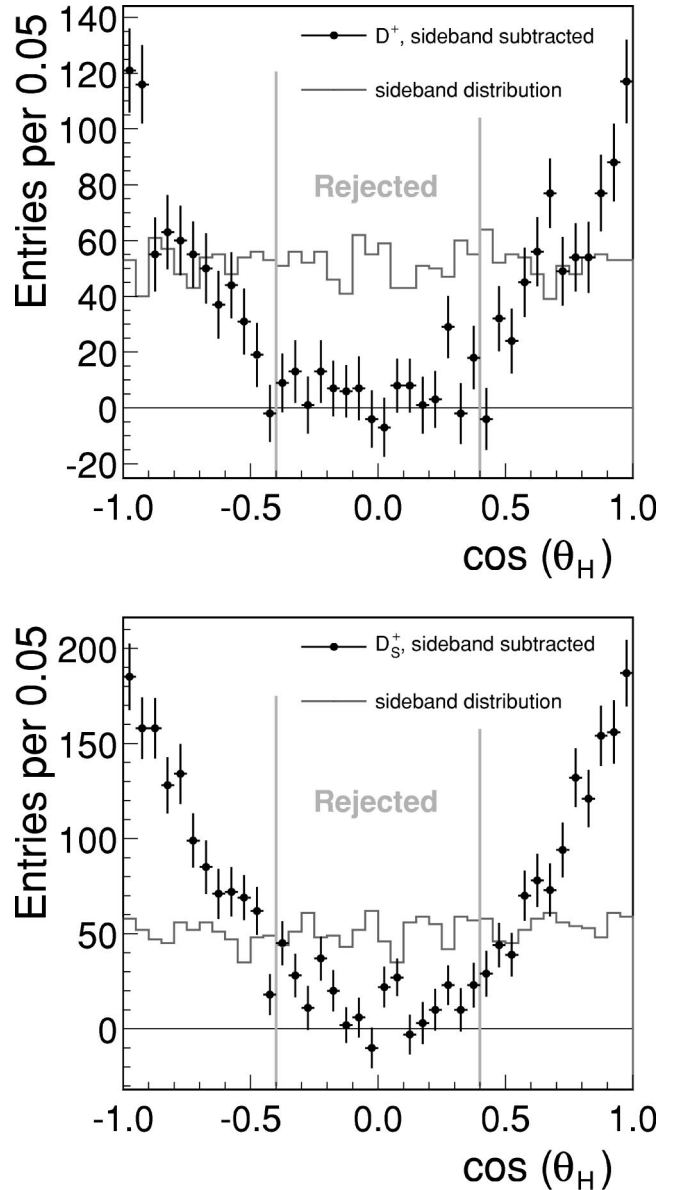

FIG. 10. Sideband subtracted and sideband distributions of the cosine of the helicity angle of the D^+ candidates (top) and D_s^+ candidates (bottom). Candidates with $|\cos(\theta_H)|$<0.4 are rejected in the selection.

$D_s^+/D^+ \rightarrow \phi\pi^+$ decays in the same event. If multiple candidates are found in an event, only the candidate with the highest $|\cos(\theta_H)|$ is considered. This procedure rejects another 9% of the underlying background.

V. MASS FITTING AND SYSTEMATIC UNCERTAINTIES

The invariant mass distribution of the $K^+K^-\pi^+$ system is fit to two Gaussian distributions and a linear background. An unbinned maximum likelihood fit is used in which the width of both Gaussian distributions, the mass of the D_s^+ and the mass difference $m(D_s^+)-m(D^+)$ are allowed to float independently. Studies of both data and Monte Carlo simulations show that a linear dependence on mass is a good de-
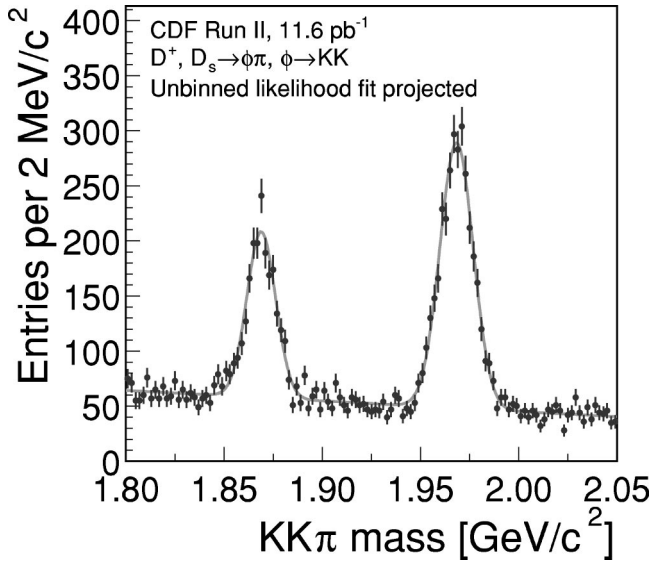
FIG. 11. Measured $K^+ K^- \pi^+$ mass distribution compared to the unbinned likelihood fit.

scription of the background. Figure 11 shows the likelihood fit superimposed onto the invariant mass spectrum. The χ^2 of the comparison of the likelihood fit to the measured mass spectrum is 127 for 118 degrees of freedom and corresponds to a χ^2 probability of 27%. The complete list of fit parameters can be found in Table II, and the fit result yields

$$m(D_s^+) - m(D^+) = 99.41 \pm 0.38 \ \text{(stat)} \ \text{MeV}/c^2. \quad (2)$$

The two charmed mesons are produced either directly in the $p\bar{p}$ collision, or they are products of a B meson decay. The trigger preferentially selects mesons with large displacements of the decay vertex from the primary interaction point. Since the D_s^+ and D^+ mesons have different lifetimes, the fraction of directly produced D_s^+/D^+ mesons to those coming from B meson decays is also different. Therefore, the momentum spectra of the two signals may differ, causing differences in the final state kinematics. This kinematic dif-

TABLE II. Likelihood fit parameter results corresponding to Fig. 11. The χ^2, number of degrees of freedom (NDF), and corresponding probability are also listed. The parameters are the mass difference (δm), the mass of the D_s^+ meson, the mass resolutions $[\sigma(D_s), \sigma(D^+)]$, the fraction of signal events $[f(D_s), f(D^+ + D_s)]$, and the slope of the background.

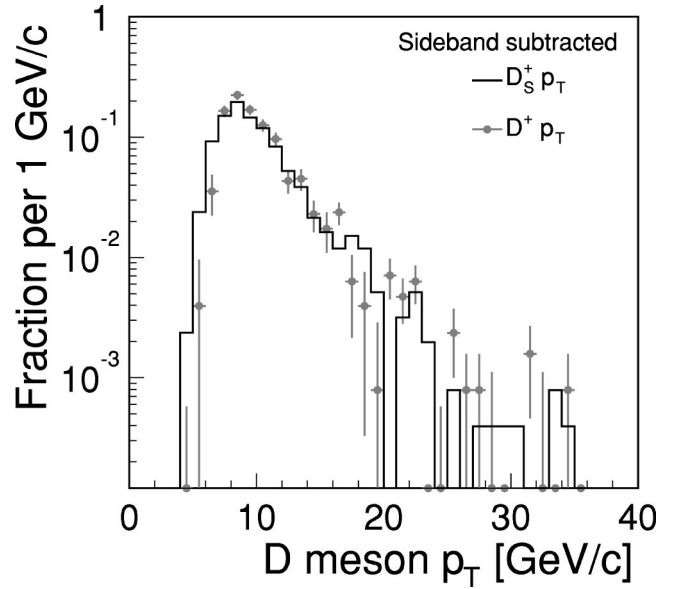| Parameter		Value
δm	$[\text{MeV}/c^2]$	99.41 ± 0.38
$m(D_s)$	$[\text{MeV}/c^2]$	1968.4 ± 0.3
$\sigma(D_s)$	$[\text{MeV}/c^2]$	8.4 ± 0.2
$\sigma(D^+)$	$[\text{MeV}/c^2]$	7.3 ± 0.3
$f(D_s)$		0.65 ± 0.01
$f(D^+ + D_s)$		0.37 ± 0.01
Background slope	$[1/\text{GeV}/c^2]$	-7.3 ± 0.7
χ^2/NDF		$126.7/118 \ (27.9\%)$

FIG. 12. Sideband subtracted distributions of the p_T of the D_s^+ candidates (solid) and D^+ candidates (dots). Both distributions are normalized such that the sum of the bins add up to one.

ference can produce a systematic shift in the measurement of the mass difference. Figure 12 shows a comparison of the p_T distributions of the D_s^+ (solid line) and D^+ (dotted line). The spectra are very similar, and we expect small systematic uncertainties.

Discussion of systematic uncertainties

The systematic uncertainties are summarized in Table III and will now be discussed in order of decreasing size. The largest single systematic uncertainty comes from fitting. To estimate the systematic uncertainties due to background modeling, the results of fits with different background models are compared. One model used in this comparison is a linear combination of orthogonal polynomials. Another model consists of two piecewise linear functions that meet at a point, which is varied between the D^+ and D_s^+ mass distributions. A systematic uncertainty of 0.08 MeV/c^2 on the mass difference is assigned based on the variation of the fit result when these different models are used. The systematic

TABLE III. Systematic uncertainty estimates for the mass difference. The total uncertainty is the quadratic sum of the individual uncertainties.

Effect	Syst. $[\text{MeV}/c^2]$
Fitting (signal+background)	0.14
Event selection	0.11
Momentum scale	0.10
Tracker effects	0.06
Calibration procedure	0.03
Total	0.21

effect due to signal modeling is studied by excluding regions of the D_s^+ and D^+ signals from the fit. In this case, a fraction of the variation of the fit result is caused by changing the statistics of the sample used. This contribution is estimated by comparing statistical uncertainties of the fit result with regions excluded to that of the fit result with no modification. After estimating the statistical contribution of the variation of the fit result, the systematic uncertainty due to signal modeling is estimated to be 0.12 MeV/c^2. These two systematic uncertainties are added in quadrature, and a systematic uncertainty of 0.14 MeV/c^2 due to fitting is obtained. This is the largest single systematic uncertainty.

To estimate the systematic uncertainty introduced by sample selection requirements, the requirements on $\chi^2(r,\varphi)$, L_{xy}, $\cos\theta_H$, and duplicate rejection are individually varied. Fit results were compared to estimate systematic effects for individual selection requirements. A fraction of the variation in the fit result is caused by statistical effects due to changing the sample composition when the selection requirements change. As before, the statistical contribution to the fit result variation is estimated from the change in the statistical uncertainty of the fit result. The only relevant selection requirement which exhibits a statistically significant effect is the cut on the $\chi^2(r,\varphi)$ variable. This variation of the mass difference is traced to an enhanced background around the D^+ mass for small values of the $\chi^2(r,\varphi)$ variable. The effect is estimated to cause a systematic uncertainty of 0.11 MeV/c^2.

The systematic uncertainty due to the momentum scale determination is estimated by analyzing a kinematically similar decay. A GEANT study is done to determine how the uncertainty in the mass difference measurement would scale with the absolute uncertainty in the $D^+ \to K\pi\pi$ mass due to momentum scale variations and shows that the uncertainty in the mass difference corresponds roughly to 11% of the absolute uncertainty on the D^+ mass. The world average mass of the D^+ meson $m(D^+) = 1869.4 \pm 0.5$ MeV/c^2 is compared to our measurement of $m(D^+) = 1868.65 \pm 0.07$ MeV/c^2 obtained in a sample of $D^+ \to K^-\pi^+\pi^+$ decays, using the same calibration procedure. To determine the absolute uncertainty of the momentum scale, the uncertainty of the world average (0.5 MeV/c^2), the statistical uncertainty of our measurement (0.07 MeV/c^2) and the difference between the two measurements (0.75 MeV/c^2) are added in quadrature. The sum in quadrature is then scaled by the factor obtained in the Monte Carlo study, and the systematic uncertainty of the momentum scale determination is estimated to be 0.10 MeV/c^2.

The mass difference is also sensitive to detector effects that are not corrected for by our calibration: namely, false curvature effects. These effects are expected to cancel in the measurement of the mass difference. As explained in the calibration section, empirical corrections of the track curvature do not completely eliminate the asymmetry of charge conjugate states. By comparing fit results with and without these empirical corrections, the systematic effect of uncorrected tracking effects is estimated to be 0.06 MeV/c^2.

The accuracy of the momentum scale calibration is limited by the size of the J/ψ sample. The systematic uncertainty on the mass difference from this limitation is estimated by individually varying the amount of material and the magnitude of the magnetic field by their statistical precisions. The two systematic effects are added in quadrature to obtain a systematic uncertainty of 0.03 MeV/c^2 due to the calibration procedure.

Finally, an explicit check is done for a systematic uncertainty caused by the difference in p_T spectra of the D_s^+ and D^+ shown in Fig. 12. The events were reweighted in the fit to make the spectra identical and the systematic effect on the mass difference is found to be negligible.

The total systematic uncertainty of the measurement is estimated by combining the above systematic uncertainties in quadrature and is found to be 0.21 MeV/c^2.

VI. SUMMARY

The difference between the mass of the D_s^+ meson and D^+ meson is measured using 11.6 pb^{-1} of data collected by CDF II and is found to be

$$m(D_s^+) - m(D^+) = 99.41 \pm 0.38 \ \text{(stat)}$$
$$\pm 0.21 \ \text{(syst)} \ \text{MeV}/c^2.$$

The result is in agreement with the current world average [7] and the most recent Babar publication of $(98.4 \pm 0.1 \pm 0.3)$ Mev/c^2 [19], with a comparable uncertainty.

[1] S. Godfrey and N. Isgur, Phys. Rev. D **32**, 189 (1985).
[2] N. Uraltsev, *Boris Ioffe Festschrift: At the Frontier of Particle Physics—Handbook of QCD*, edited by M. Schifman (World Scientific, Singapore, 2001), Vol. 3, p. 1577.
[3] A. V. Manohar and M. B. Wise, Monogr. Part. Phys. Nucl. Phys. Cosmol. **10**, 102 (2000).
[4] R. Lewis and R. M. Woloshyn, Nucl. Phys. B (Proc. Suppl.) **93**, 192 (2001).

[5] R. Lewis and R. M. Woloshyn, Phys. Rev. D **58**, 074506 (1998).

[6] J. Hein *et al.*, Phys. Rev. D **62**, 074503 (2000).

[7] Particle Data Group, K. Hagiwara *et al.*, Phys. Rev. D **66**, 010001 (2002).

[8] The D_s^+, D^+, and D^0 notation used in the text also implies the charge conjugate states.

[9] W. Ashmanskas *et al.*, Nucl. Instrum. Methods Phys. Res. A **447**, 218 (2000).

[10] R. Blair *et al.*, "The CDF-II detector: Technical design report," Report No. FERMILAB-PUB-96-390-E.

[11] T. K. Nelson *et al.*, Report No. FERMILAB-CONF-01/357-E.

[12] A. Sill *et al.*, Nucl. Instrum. Methods Phys. Res. A **447**, 1 (2000).

[13] T. Affolder *et al.*, Nucl. Instrum. Methods Phys. Res. A **485**, 6 (2002).

[14] K. T. Pitts *et al.*, Report No. FERMILAB-CONF-96-443-E.

[15] W. Ashmanskas *et al.*, Report No. FERMILAB-CONF-02/035-E.

[16] A. Bardi *et al.*, Nucl. Instrum. Methods Phys. Res. A **485**, 178 (2002).

[17] E. J. Thomson *et al.*, IEEE Trans. Nucl. Sci. **49**, 1063 (2002).

[18] R. Brun, R. Hagelberg, M. Hansroul, and J. C. Lassalle, Report No. CERN-DD-78-2-REV; Report No. CERN-DD-78-2.

[19] B. Aubert *et al.*, Phys. Rev. D **65**, 091104(R) (2002).